Inorganic Chemistry

Article

pubs.acs.org/IC

Toward a Small Molecule, Biomimetic Carbonic Anhydrase Model: Theoretical and Experimental Investigations of a Panel of Zinc(II) Aza-Macrocyclic Catalysts

Lucas Koziol, Carlos A. Valdez, Sarah E. Baker, Edmond Y. Lau, William C. Floyd, III, Sergio E. Wong, Joe H. Satcher, Jr., Felice C. Lightstone,* and Roger D. Aines*

Lawrence Livermore National Laboratory, 7000 East Avenue, Livermore, California 94550, United States

Supporting Information

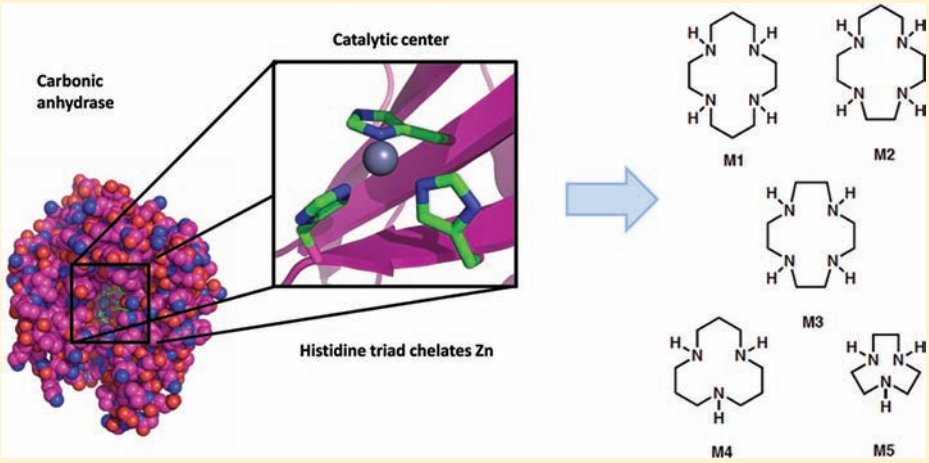

ABSTRACT: A panel of five zinc-chelated aza-macrocycle ligands and their ability to catalyze the hydration of carbon dioxide to bicarbonate, $H_2O + CO_2 \rightarrow H^+ + HCO_3^-$, was investigated using quantum-mechanical methods and stopped-flow experiments. The key intermediates in the reaction coordinate were optimized using the M06-2X density functional with aug-cc-pVTZ basis set. Activation energies for the first step in the catalytic cycle, nucleophilic CO_2 addition, were calculated from gas-phase optimized transition-state geometries. The computationally derived trend in activation energies was found to not correspond with the experimentally observed rates. However, activation energies for the second, bicarbonate release step, which were estimated using calculated bond dissociation energies, provided good agreement with the observed trend in rate constants. Thus, the joint theoretical and experimental results provide evidence that bicarbonate release, not CO_2 addition, may be the rate-limiting step in CO_2 hydration by zinc complexes of aza-macrocyclic ligands. pH-independent rate constants were found to increase with decreasing Lewis acidity of the ligand-Zn complex, and the trend in rate constants was correlated with molecular properties of the ligands. It is suggested that tuning catalytic efficiency through the first coordination shell of Zn^{2+} ligands is predominantly a balance between increasing charge-donating character of the ligand and maintaining the catalytically relevant pK_a below the operating pH.

1. INTRODUCTION

The sequestration of gaseous CO_2 into the aqueous or solid phase is accomplished by carbonic anhydrase (CA) in animals[1−5] and by RuBisCO in plants.[6,7] In most mammals, the predominant CA contains a Zn^{2+} center and regulates pH via the equilibrium $CO_2 \rightleftharpoons HCO_3^-$. The active site is composed of one zinc atom coordinated to three histidines. A fourth coordination site is occupied by a water molecule, which is loosely bonded through its oxygen (Figure 1). The electronic properties of the histidines, as well as multiple nonbonded interactions provided by polar residues near the catalytic center (e.g., Thr199), decrease the pK_a of the Zn-bound water to about 7.[8] CA thus provides a nucleophilically "active" hydroxide at biological pH (about 7.4).

The key steps in the catalytic cycle are given in Figure 3. Zn^{2+} and the catalytic water are shown explicitly. L refers to a first coordination shell (such as CA or, in this work, M1−M5). The number of coordinating ligand atoms can vary (shown is 3) between 3 and 5. The cycle is divided into three steps. In CO_2 addition (Step I), Zn-bound hydroxide reacts with CO_2 to form Zn-bound bicarbonate. Bicarbonate release (Step II) is a substitution in which a solvent water replaces bicarbonate to

Received: March 9, 2012
Published: June 6, 2012

   dx.doi.org/10.1021/ic300526b | *Inorg. Chem.* 2012, 51, 6803−6812

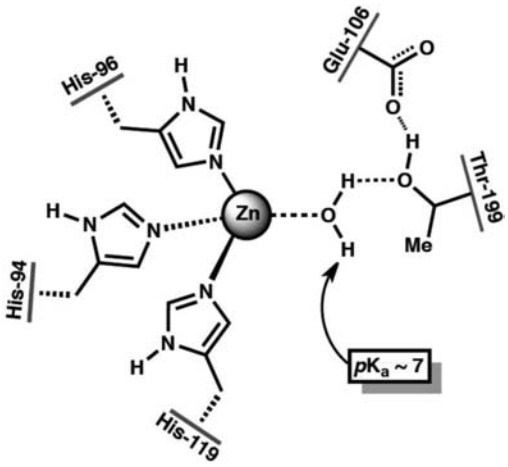

Figure 1. Active site of human carbonic anhydrases features a first coordination shell of three histidine residues and an activated water molecule. In addition, H-bond interactions (Thr199 shown) play an important role in determining enzyme activity.

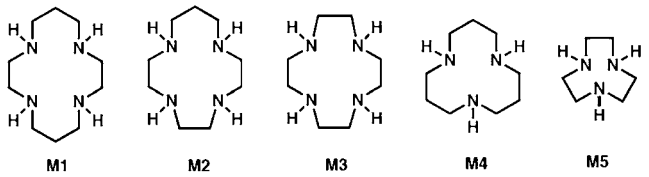

Figure 2. Five aza-macrocyclic ligands considered in this work. Hydrogens bonded to carbon are omitted for clarity. M1 = 1,4,8,11-tetraazacyclotetradecane or [14]aneN4 or Cyclam. M2 = 1,4,7,10-tetraazacyclotridecane or [13]aneN4. M3 = 1,4,7,10-tetraazacyclododecane or [12]ane4 or Cyclen. M4 = 1,5,9-triazacyclododecane or [12]aneN3. M5 = 1,4,7-triazacyclononane or [9]aneN3.

regenerate the catalyst in protonated form. Step III, deprotonation of the water molecule, is required to regenerate the active hydroxide form. Step III is known to be the rate-limiting step in CA enzymes,[9,10] involving an extended water network (over 8−10 Å)[11] to shuttle the excess proton from the active site into bulk solvent. In small-molecule catalysts, the catalytic center is open to the solvent, and Step III is expected to be fast.

Several theoretical and experimental studies have addressed the catalytic cycle of CA and model systems. Particularly, numerous studies have focused on the nature of the bicarbonate coordination to Zn, and its effects on catalysis rate. Anders and co-workers identified the relative minima and saddle points for the complex $(NH_3)_3$−Zn^{2+}−(OH^-) + CO_2 using density functional theory (DFT).[12] They found a five-coordinate Zn atom containing bicarbonate and a water molecule, and a facile intramolecular proton transfer from the water to form carbonic acid, which is a better leaving group than bicarbonate. The (NH_3) groups had significant flexibility to orient around the Zn atom, which is not the case with the secondary amines confined to a ligand ring. Molecular dynamics simulations of CA active site by Merz and co-workers found that a bidentate bicarbonate coordination was the global minimum.[4] In addition, this minimum stabilized a long-lived water molecule that is poised for nucleophilic substitution of the bicarbonate. Experimental studies on a series of tris(pyrazolyl)hydroborate Cd^{2+} ligands suggested that unidentate bicarbonate binding modes are preferred, and that the degree of unidentate character with metal substitution correlated with activity in the corresponding metal-substituted CAs.[13] Early X-ray crystal structure showed monodentate binding in HCAI[14] and pseudobidentate binding in the Thr200 → His mutant of HCAII.[15] Typically, isolation of the bicarbonate intermediate in highly active CA enzymes is unfeasible because of the extremely fast kinetics. CA is one of the fastest enzymes known, with rate constant on the order of 10^6 M^{-1} s^{-1}.[16] We note that a significant amount of this activity depends on nonbonded atoms not directly coordinated to the zinc, especially Thr199 and Glu106 (Figure 1). Lindskog and co-workers showed that the Thr199 → Ala mutant had a 100× reduction in CO_2 hydration activity compared to the native enzyme, as well as increasing the pK_a of the zinc-bound water by 1 unit.[17] Interestingly, mutating Glu106 → Ala or Gln leads to a 1000× reduction in activity compared to the native enzyme. A possible explanation is that without the presence of the glutamic acid (Figure 1), Thr199 is free to act as an H-bond acceptor to the Zn-bound HCO_3^- anion, therefore stabilizing the bicarbonate and preventing effective substitution by water, which is a weak nucleophile.[17]

A fair amount of previous work has focused on inorganic, metal-binding ligands in the context of CO_2 binding or conversion.[18−25] Detailed experimental studies on two prototypical aza-macrocycles have been reported by van Eldik and co-workers.[18,19] These studies were of great importance in establishing the validity of the small-molecule biomimetic concept. Importantly, Kimura and others showed that plotting the rate constants as a function of pH follows a sigmoidal curve, with an inflection point exactly at the water pK_a.[19] They established that only the deprotonated (hydroxide) form is catalytically active, consistent with a nucleophilic addition mechanism. Those two ligands, tetraaza-cyclo[12]ane (M3),[19] and triaza-cyclo[12]ane (M4),[18] are included in this work. In addition, M2 and M5 in this work are reported for the first time in the context of CO_2 catalysis.

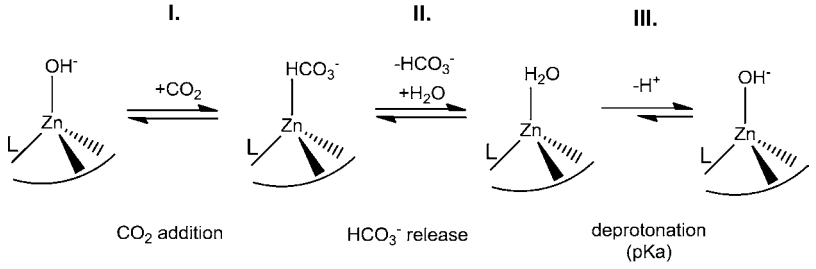

Figure 3. Catalytic cycle divided into three reactions: I, CO_2 addition; II, bicarbonate release; and III, deprotonation of the water molecule.

dx.doi.org/10.1021/ic300526b | Inorg. Chem. 2012, 51, 6803−6812

In this paper, we studied five aza-macrocycle ligands as model systems to develop an understanding of the ligand properties that influence CO_2 hydration. The ligands are shown in Figure 2. They are ordered M1−M5 by decreasing Zn−O bond length of the hydroxide-bound complex (at the M06-2X/aug-cc-pVTZ level). Throughout this work, the following abbreviations are used. M^{2+} = L-Zn^{2+}; M-X = L-Zn^{2+}-X, where X can equal OH^-, H_2O, or HCO_3^-. Key geometrical parameters for M1−M5 are shown in Figure 4. Full Cartesian coordinates

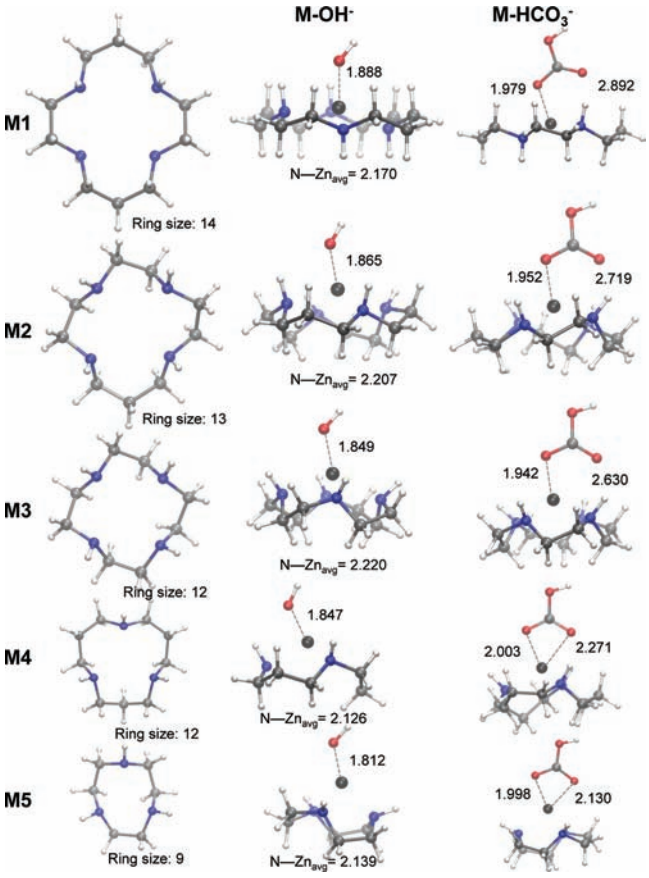

Figure 4. Equilibrium geometries of M-OH^- and M-HCO_3^- at the M06-2X/aug-cc-pVTZ level. *Left:* top view of ligands M1−M5 at M-OH^- frozen structure. Zn and OH have been omitted for clarity. *Center:* side view of M-OH^-. The Zn−O bond length is labeled as well as average Zn−N bond length. *Right:* side view of M-HCO_3^-. Both Zn−O interatomic distances are labeled. M1−M3 adopt monodentate HCO_3^- binding modes, while M4−M5 have bidentate modes, with two Zn−O distances less than 2.3 Å. All distances are in Angstroms.

and energies for all complexes studied here are given in the Supporting Information. The ligands differ by the number of methylene groups in the ring, and by having either three or four metal-coordinating nitrogens.

2. MATERIALS AND METHODS

Computational Details. Fully optimized geometries of M^{2+}, M-H_2O, M-OH^-, and M-HCO_3^- were obtained for M1−M5 using DFT. Geometries for M-OH^- and M-HCO_3^- are shown in Figure 4. For all minimizations, the M06-2X functional[26] was used with the aug-cc-pVTZ basis set.[27] Only the lowest-energy conformers were considered in this work. The conformational search and trends in energies were found by creating initial ligand geometries in various eclipsed and staggered conformations using automated scripts and manually, and by starting geometry optimization from these structures. Truhlar and co-workers showed that M05 and M06 functionals characterized for main group elements, rather than transition metals, more accurately replicated CCSD equilibrium geometries and properties.[28] This is owed to Zn having a fully filled d^{10} shell, which also leads to zero spin−orbit coupling. Scalar relativistic effects were not treated, although they may provide a nontrivial systematic correction to the Zn lengths.[28] In the calculation of the activation energies, basis-set superposition error between CO_2 and the complex was accounted for at the optimized geometries using the counterpoise-correction.[29] Because of the large basis set and similarity in the series M1−M5, this correction was found to be small (average 0.5 kcal/mol) and similar for all compounds. Optimizations of all ligands was performed using NWChem 6.0.[30]

Transition state calculations and pK_a calculations were carried out using smaller basis sets, because of the expense of harmonic frequency calculations. To optimize transition states, the 6-311+G(d,p) basis set was used for all atoms except Zn. For Zn, the B2 basis set of Truhlar and co-workers, was used.[28] The geometries were verified to have one negative eigenvalue by a frequency calculation. Additionally, intrinsic reaction coordinate (IRC) calculations starting from the optimized transition states were performed. These confirmed that the minimum-energy path connected Zn-bound HCO_3^- and the association complex. All basis sets for Zn were obtained from the EMSL Basis Set Library.[31,32]

To the best of our knowledge, pK_as associated with deprotonation of the Zn-bound water has been reported for only three of the five compounds, M1,[33] M3,[19,33] and M4.[18,19] Since the pK_a can significantly affect observed rates under given conditions, we determined the pK_a values for M2 and M5. These were calculated using two methods. (1) Linear fitting to the known pK_as using a single fitting parameter, followed by interpolation. The chosen parameter was the Zn−O distance in the M-OH^- species. (2) As a second, independent method, aqueous-phase pK_a values were estimated using electronic structure calculations and the thermodynamic cycle shown in Figure 5.[34,35] Because of computational expense of frequency

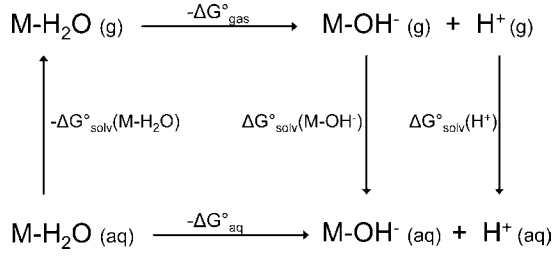

Figure 5. Reaction cycle used to estimate the trend in aqueous-phase pK_a from ab initio calculations.

calculations, free-energy corrections to ΔU were calculated using a smaller triple-ζ basis set, 6-311+G(d) at the corresponding minima. Free energies of solvation, ΔG_{solv}, were calculated from single-point calculations at gas-phase geometries using the SMD model,[36] which is specifically parametrized for solvation free energies. This model does use experimental values, particularly, $\Delta G_{solv}(H^+)$ and $G_{gas}(H^+)$, which were taken to be −264.61 kcal/mol and −6.28 kcal/mol, respectively.[34] Transition state and pK_a calculations, including

dx.doi.org/10.1021/ic300526b | Inorg. Chem. 2012, 51, 6803−6812

SMD single-point solvation energies at gas-phase optimized geometries, were carried out using Gaussian 09.[37]

Materials. All reagents used were of analytical grade, were purchased from commercial suppliers, and were used as received. Cyclam ([14]aneN4, M1) and M2 ([13]aneN4) were purchased from Alfa Aesar (Ward Hill, MA). M4 ([12]aneN3) and M5 ([9]aneN3) were purchased from TCI Chemicals (Portland, OR), while Cyclen ([12]aneN4, M3) was purchased from Strem Chemicals (Newburyport, MA). ^{1}H NMR (400 MHz) and ^{13}C NMR (125 MHz) spectra of the complexes were recorded in D_2O unless otherwise specified with a Bruker Avance AVB-400 nuclear magnetic resonance (NMR) spectrometer equipped with a 5 mm z-gradient broadband probe. The NMR spectra for complexes, M3-Zn^{2+}[38] and M4-Zn^{2+}[33] were satisfactory and matched the ones published in the literature. Data are presented as follows: chemical shift (parts per million, ppm), multiplicity s = singlet, t = triplet, quin = quintet, m = multiplet, br = broad, coupling constant J (in Hz). Elemental analyses to further confirm their composition and purity were obtained at the LLNL Microanalytical Facility.

General Procedure for Complex Preparation. The azamacrocycle (1.0 g, 5−7.5 mmol) is dissolved in ethanol (10 mL) in a scintillation vial equipped with a stir bar. The colorless solution is heated and stirred at 65 °C using an oil bath. Zinc(II) perchlorate hexahydrate ($Zn(ClO_4)_2{\cdot}6H_2O$ (1.2 equivalents to azamacrocycle) is dissolved in ethanol (3 mL), and this colorless solution is slowly added to the azamacrocycle at 65 °C dropwise. Upon zinc addition, the colorless mixture becomes turbid and eventually a white precipitate forms. The suspension is stirred at 65 °C for 2 h. In some cases (M3 and M1), the suspension becomes a solution, but upon standing at ambient temperature, the white precipitate reforms. In other cases, even at 65 °C, the white precipitate remains and upon cooling of the mixture, it is filtered and washed with cold ethanol (3 × 30 mL). The resulting white solid (with the exception of M4, in which case the solid was tan-colored) was dried under vacuum over two days at ambient temperature.

M1-Zn(II) Complex. The complex was synthesized as described above in the general procedure and obtained as a white, flaky solid (95%). ^{1}H NMR (400 MHz, D_2O, mixture of conformers) δ 3.60−3.58 (br s, 1H), 3.32−3.29 (br s, 1H), 3.20−3.11 (m, 5H), 3.06−3.03 (m, 1H), 2.95−2.91 (m, 3H), 2.85−2.78 (m, 4H), 2.72−2.69 (m, 1H), 2.64−2.60 (m, 1H), 2.51−2.45 (m, 1H), 1.97−1.89 (m, 1H), 1.80−1.75 (m, 1H), 1.73−1.60 (m, 1H); ^{13}C NMR (125 MHz, mixture of conformers) δ 50.6, 50.5, 50.1, 49.2, 49.0, 47.8, 46.5, 46.4, 46.1, 46.0, 28.0, 27.5, 27.5, 23.7. Anal. ($C_{10}H_{24}N_4Zn{\cdot}2ClO_4{\cdot}H_2O$) C, H, N.

M2-Zn(II) Complex. The complex was synthesized as described above in the general procedure as a white, flaky solid (93%). ^{1}H NMR (400 MHz, D_2O, major conformer) δ 3.50−3.48 (br s, 1H), 3.15−3.10 (m, 4H), 2.84−2.72 (m, 6H), 1.92−1.90 (m, 1H), 1.73−1.71 (m, 1H); ^{13}C NMR (125 MHz, major conformer) δ 50.1, 48.0, 45.5, 43.7, 27.2. Anal. ($C_9H_{22}N_4Zn{\cdot}2ClO_4{\cdot}H_2O$) C, H, N.

M3-Zn(II) Complex. The complex was synthesized as described above in the general procedure as a white, granular solid (95%). ^{1}H NMR (400 MHz, D_2O, major conformer) δ 2.97−2.93 (m, 8H), 2.85−2.79 (m, 8H); ^{13}C NMR (125 MHz) δ 43.7. Anal. ($C_8H_{20}N_4Zn{\cdot}2ClO_4{\cdot}2H_2O$) C, 21.24; H, 4.88; N, 12.33; Found: C, 20.33; H, 5.12; N, 11.86.

M4-Zn(II) Complex. The complex was synthesized as described above in the general procedure as a tan-colored solid (89%). ^{1}H NMR (400 MHz, D_2O, major conformer) δ 2.77 (t, J = 6.0, 12H), 1.66 (quin, J = 6.0, 6H); ^{13}C NMR (125 MHz, major conformer) δ 46.7, 24.9. Anal. ($C_9H_{21}N_3Zn{\cdot}2ClO_4{\cdot}H_2O$) C, 28.83; H, 5.11; N, 9.26; Found: C, 23.94; H, 4.98; N, 9.60.

M5-Zn(II) Complex. The complex was synthesized as described above in the general procedure as a white, granular solid (92%). ^{1}H NMR (400 MHz, D_2O) δ 2.96−2.95 (br m, 6H), 2.73−2.71 (br m, 6H); ^{13}C NMR (125 MHz, D_2O) δ 42.9. Anal. ($C_6H_{15}N_3Zn{\cdot}2ClO_4{\cdot}H_2O$) C, H, N.

Stopped-Flow Measurements. Experimental catalytic rate constants for the CO_2 hydration reaction catalyzed by five Zn containing azamacrocycles were determined using stopped-flow spectrophotometry using methods similar to those previously described.[19] All chemicals were purchased from Sigma-Aldrich and used as purchased. Prior to the experiment, a solution of CO_2 saturated water was prepared by sparging deionized water with 100% CO_2 gas at 25 °C for at least 30 min. Using Henry's constant, this solution was calculated to contain 33.8 mM [CO_2]. Additionally, a solution containing 0.2 M $NaClO_4$, 0.1 M AMPSO buffer, and 5×10^{-5} M thymol blue indicator, pH 9.0 (adjusted using H_2SO_4), was evacuated under vacuum for 1 h followed by sparging with nitrogen for 20 min to remove dissolved CO_2. A baseline uncatalyzed rate was found by rapidly mixing the dissolved CO_2 solution and the buffer solution 1:1 in an Applied Photophysics stopped-flow spectrophotometer while recording the time-dependent absorbance at λ = 596 nm. Twenty milliliters of 1 mM solution of each azamacrocycle in the AMPSO buffer solution were prepared by stirring under nitrogen. The catalyst concentration-dependent initial rates were found by performing dilutions of the 1 mM solutions with AMPSO buffer solution. Initial rates for each catalyst concentration were calculated by fitting the first 10% of the time-dependent absorbance data with a single exponential decay function. All kinetic runs were performed for 100 s to ensure that equilibrium was reached and that the final absorbance value was indicative of reaction completion. Therefore, the time period for fitting the initial rates could be accurately defined for each reaction. Each concentration of catalyst was measured four times, and the standard deviation determined. Initial rates were calculated using the equation

$$v_{init} = Q(A_0 - A_e)[d(\ln(A - A_e))/dt]_{t\to 0} \quad (1)$$

where Q is the buffer factor which was determined experimentally by titrating the AMPSO buffer solution with three concentrations of HCl in the stopped-flow spectrophotometer, and A_0 and A_e were the initial and final absorbance values, respectively. The value of Q measured was −0.29. It was determined by mixing the AMPSO buffer solution 1:1 with three different HCl/water solutions and measuring the absorbance in the stopped flow spectrophotometer. The HCl concentrations measured were 0.0076, 0.0153, and 0.031 M, and were chosen to represent a range of [H^+] similar to the [H^+] generated in the CO_2 hydration reaction. The rate constant k_{obs} for each of the macrocycles was determined as the slope of v_{init}/CO_2 vs macrocycle, and the error was calculated as the deviation of the curve from linearity.

Experimental pK_a Determination. pK_a values for M2 and M3 were determined experimentally using a Metrohom 800 dosimeter using Tiamo 2.2 software for data analysis. Briefly,

dx.doi.org/10.1021/ic300526b | Inorg. Chem. 2012, 51, 6803−6812

100 mg (0.2 mM) of the zinc-complexed aza-macrocycle was dissolved in 2 mL of 0.1 M $HClO_4$ and stirred at 25 °C. To this solution was added 10 mL of 0.1 M NaOH at a rate of 0.2 mL/minute while the pH was monitored to identify half-equivalence points.

3. RESULTS AND DISCUSSION

Equilibrium Geometries of Lowest-Energy Conformers. The optimized geometries for M-OH^- species are given in Figure 4. For M2−M5, the lowest-energy conformer contains all "up" facing N−H bonds, located on the same side of the ring as the Zn−O bond. In M1, the lowest-energy structure contains two up and two down N−H bonds. Interestingly, the all-up conformer for M1 was found to be only 1.55 kcal/mol higher in energy than the two-up and two-down conformer. In contrast, higher ring conformations for M2−M5 were typically spaced by 3 or more kcal/mol. The presence of multiple conformers for M1 was further confirmed by NMR analysis. In the case of M1, the ^{1}NMR showed the predominance of one conformer over another, thus supporting the notion that this complex may exist in discernible conformations in aqueous solution at ambient temperature. The presence of multiple conformers of metal-coordinated azamacrocycles has been reported before, and their distribution depends strongly on factors such as temperature and ionic strength.[39]

Typically, N−H bond up configurations are found to be consistently favored energetically, as this geometrical arrangement minimizes steric repulsions between alkyl groups on the ring and the lone pairs of the oxygen atoms. One of the exceptions to this trend seems to be M1, which accommodates the metal almost in the ring plane, so neither side of the ring sees higher stabilization. The resulting complex is effectively planar (Figure 4). A thorough analysis of the conformational spectrum of aza-macrocycles is beyond the scope of this work. However, we note that low-energy conformers adopted both chair and boat configurations in their 6-membered ring state (Figure 6). The 4-coordinated rings have chair conformations. In the 3-coordinate M4, the smaller ring area leads to destabilization of chair conformations because steric repulsions between adjacent rings are increased because of proximity, leading to boat conformations where the methylene group (para to the Zn atom) faces up away from the area under the ring (Figure 6). None of the complexes accepted a second water molecule into their coordination shell from their M-OH^- complex, on the basis of attempted gas-phase optimizations. Only M1 accepted a second water molecule in its M1-H_2O complex, on opposite side of the ring, in accordance with crystal structures.[24]

The ligands are ordered in decreasing Zn−O bond lengths in the M-OH^- species from M1−M5 (Table 1). This bond length correlates with the size of the ring (Figure 4). In the M-OH^- complexes, the Zn−O bond length is 1.888 Å in M1 (14 atoms), and 1.812 Å in M5 (9 atoms). M3 and M4 both have rings containing 12 atoms and have very similar bond lengths (1.849 and 1.847 Å, respectively), even with different number of coordinating nitrogens. There is a 2-fold implication with regards to considering bond lengths. One, the size of the ligand directly influences the Zn−O bond length. Two, this effect should correlate with the Lewis acidity of the overall complex caused by the electron-donating nature of the ligand. Equilibrium values for these bond lengths are given in Table 1.

Table 1. Calculated Zn−O Bond Lengths at Equilibrium M06-2X/aug-cc-pVTZ Geometries for M-OH^-, M-HCO_3^-, and M-H_2O[a]

	M-OH^-	M-HCO_3^-	M-H_2O
M1	1.888	1.979	2.147
M2	1.865	1.952	2.094
M3	1.849	1.942	2.061
M4	1.847	2.003/2.271	2.061
M5	1.812	1.998/2.130	1.988

[a]Forward slashes indicate bidentate binding modes; both interatomic distances are given. All values are in Å.

The optimized geometries for M-HCO_3^- are shown in Figure 4. They were calculated with the same ring conformations as M-OH^-. In all cases, the lowest-energy orientation of HCO_3^- feature the sp^2 oxygen facing down toward the ring, and the −OH moiety facing up perpendicular to the ring plane (for example, the Lipscomb orientation).[40] The four-coordinate complexes had unidentate binding modes, where only one oxygen is within 2.3 Å of the Zn, while M4 and M5 had bidentate structures, with two Zn−O distances shorter than 2.3 Å (Table 1).

Determination of the pK_a of the Zn-Bound Water Molecule. The pK_a of three of the compounds has been previously reported in experimental studies, pK_a(M1) = 9.8,[33] pK_a(M3) = 7.9,[19,33] and pK_a(M4) = 7.3.[18,19] The remaining two (M2 and M5) have, to the best of our knowledge, not been reported so far. Indirectly (from HPLC transesterification measurements), it appears that the pK_a of M5 is below 7.[41] However, direct titrations were difficult to achieve because of the tendency of the compound to precipitate above pH 7.[33] A pK_a below about 8 will have negligible effects on the discussions below. A least-squares fit to the known pK_as yields,

$$pK_a = 55.459(l_{Zn-O}) - 94.893 \quad (2)$$

where M-OH^- complexes were used because they gave the highest R^2 (0.965). The general methodology of fitting a pK_a to a single bond length has recently been extensively benchmarked for different classes of compounds.[42,43] Surprisingly, high accuracy (e.g., within 0.2 pK_a units) can be attained if the test set is sufficiently closely correlated. Using the fit in eq 2,

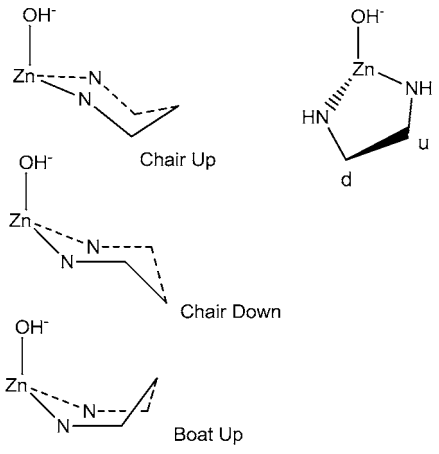

Figure 6. Observed binding motifs in low-energy conformers of M-OH^-. *Left:* Low-energy conformations adopted in the 6-membered rings. *Right:* Only one conformation was found for ligands in 5-membered rings.

dx.doi.org/10.1021/ic300526b | Inorg. Chem. 2012, 51, 6803−6812

pK_a(M2) = 8.6 and pK_a(M5) = 5.6. Independently, these pK_as were also calculated using the thermodynamic cycle shown in Figure 5. This method had no empirical parameters, and its results could be compared to the known pK_a values. Previous benchmarks for this model have reported root-mean-square errors for aqueous pK_as of about 0.4−0.8 units.[34,35] The order of the three known pK_a's was reproduced correctly, also the ordering of all five pK_a's was the same as using the interpolation method. However, a mean difference between the calculated and the experimental pK_a's of +0.823 pK_a units was found. This value is within the benchmarked error of the DFT thermodynamic cycle method. The resulting pK_as are listed in Table 2. They differ by 0.3 units from M3 and M4, and by 0.7 units from M1. We were also able to measure the pK_a experimentally for M2 and M3, as described in the Experimental section. For M3, we obtained a pK_a of 8.1, in agreement with previously reported values. For M2, we obtained 8.32. The experimental value for M2 obtained in this work is in fairly good agreement with the interpolated value of 8.6. However, the calculated value using the thermodynamic cycle of 8.9 has a larger error of 0.6 pK_a units, even after correcting for systematic error. For the purposes of the following discussion, particularly deriving pK_a-independent rate constants from pH 9.0 rates, the values of 8.3 and 5.6 are used for M2 and M5, respectively.

Table 2. Experimentally Determined[18,19,33] and Calculated pK_as for M1−M5[a]

	exp. (previous)	exp. (this work)	interpolated	DFT/therm. cycle
M1	9.8		9.8	10.5
M2		8.3	8.6	8.9
M3	7.9	8.1	7.7	7.6
M4	7.3		7.6	7.0
M5			5.6	4.3

[a]The center column (interpolated) was used to obtain k_{ind} from k_{obs} according to eq 5.

Observed Rate Constants. The experimentally observed rate constants, k_{obs}, at 25 °C and pH 9.0 are listed in Table 3 and plotted in Figure 7. From the data obtained, M3 has the highest catalytic activity with a rate constant of 2493 M^{-1} s^{-1}, in good agreement with previously reported values of 2649 and 3012 M^{-1} s^{-1} at pH 8.83 and 9.11, respectively.[19] The least active compound was found to be M5, which was practically noncatalytic with a rate constant of 88 M^{-1} s^{-1}.

Table 3. Observed k_{obs} and pH-Independent k_{ind} Rate Constants and Standard Deviations σ[a]

	k_{obs}	k_{ind}	σ_{obs}	σ_{ind}
M1	689.5	5039.7	126.7	926.2
M2	1877.4	2278.8	99.2	120.4
M3	2493.5	2691.5	48.9	52.8
M4	1082.6	1104.2	204.8	208.9
M5	88.3	88.3	66.1	66.2

[a]Units are M^{-1} s^{-1}.

As shown by van Eldik and others, only the M-OH^- form of the aza-macrocycle complex participates in CO_2 and ester hydrolysis reactions.[19,44] Therefore, experiments performed at a pH of within 1 unit of the pK_a will contain significant fractions of the protonated, inactive form. To compare rate constants independently of catalyst pK_a, observed rate constants, k_{obs}, must be converted to their analogous, pH-independent form, k_{ind}.

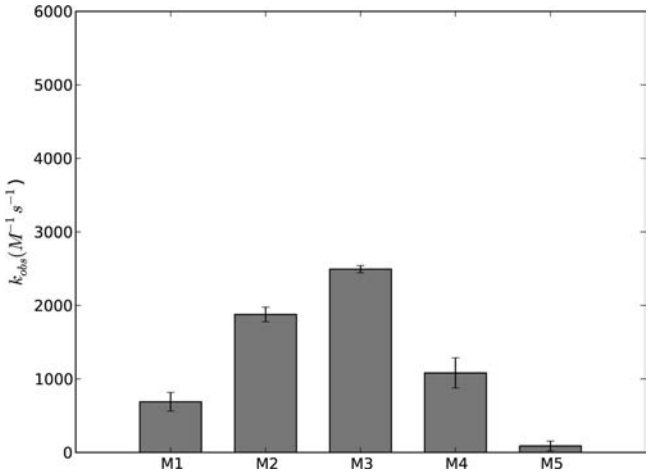

Figure 7. Experimentally observed rate constants, k_{obs}, for M1−M5, at 25 °C and pH 9.0.

Conversion between observed and pH-independent rates was performed as follows, following equivalent derivation for aza-macrocycle rate constants by other authors.[45] Total concentration of catalyst equals $[M_{tot}] = [M\text{-}OH^-] + [M\text{-}H_2O]$. The observed rate constant is given by,

$$v_{init} = k_{obs}[M_{tot}][CO_2] \quad (3)$$

where v_{init} is measured initial velocity. The pH-independent rate constant is

$$v_{init} = k_{ind}[M\text{-}OH^-][CO_2] \quad (4)$$

Combining the two equations yields,

$$k_{ind} = k_{obs}\frac{[M_{tot}]}{[M\text{-}OH^-]} = k_{obs}(1 + 10^{pKa-pH}) \quad (5)$$

The conversion factor between rate constants equals the fraction of deprotonated species, which is obtained using the Henderson−Hasselbalch equation.

The pH-independent rate constants obtained from eq 5 are listed in Table 3 and plotted in Figure 8. The ordering of the rate constants remains the same except for M1, which has $k_{ind} \gg k_{obs}$ because of its high pK_a. An interpretation of k_{ind} is that it should equal k_{obs} when pH ≫ catalyst pK_a. Table 3 suggests that at higher operating pH (e.g., above 10.8), M1 may have significantly higher observed activity than at pH 9. However, this awaits experimental confirmation, as other factors, including distribution of low-energy conformations and catalyst oligomerization with carbonate, may be important. While this finding may be of limited utility in many biological applications because of the high pH requirements, many amine catalysts currently used in industrial CO_2 sequestration operate at pH well above 11.[46]

The ordering of k_{ind} correlates fairly well with the order of calculated Zn−O bond lengths, so that k_{ind} increases with increasing Zn−O bond length. The only deviation from this trend was between M2 and M3, which are switched. This could be a result of the close proximity of the statistical errors associated with the measurements. In addition, it could be the result from use of the interpolated pK_a, which introduces additional error. We also note that M4 has signicantly lower

dx.doi.org/10.1021/ic300526b | Inorg. Chem. 2012, 51, 6803−6812

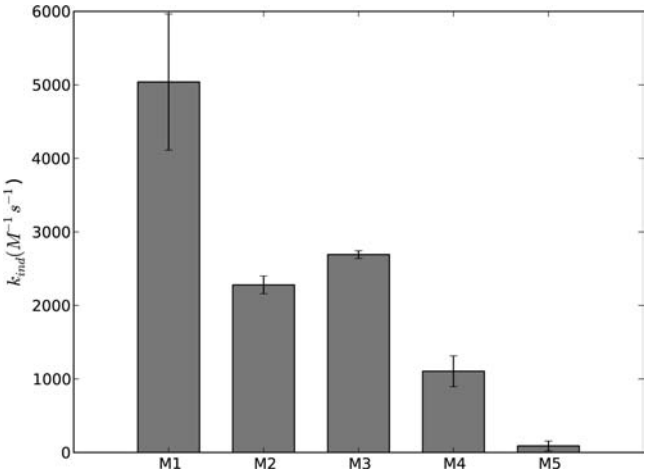

Figure 8. Experimental pH-independent rate constants, k_{ind}, obtained from k_{obs} using eq 5.

activity than M3, despite only a slightly shorter bond length. The decreased activity is likely due to having less coordinating atoms in M4 than M3; this likely provides decreased charge donation into Zn which is not reflected in the Zn−O length (possibly due to steric hindrance by the larger ring). Partial atomic charges on the Zn were also calculated from the DFT wave function with the restricted electrostatic potential (RESP) fitting method implemented in NWChem. These calculations showed that 4-coordinate ligands had lower Zn charge than 3-coordinate ligands, which confirms the geometrical trend suggesting lower Zn acidity with 4-coordinate compounds. Overall, increasing the Zn−O bond length in the M-OH^- complexes appears to be a good indicator of pH-independent rate constants and can be used in computationally aiding the design of novel catalysts. Previous studies have found a correlation between increased catalyst pK_a and higher rate constants, in line with the trend found here.[19]

Interestingly, we note that 4-coordinate complexes demonstrate higher activity than 3-coordinate complexes. The 4-coordinate complexes have monodentate ground-state HCO_3^- binding modes, while 3-coordinate complexes allow bidentate binding modes. This provides evidence that monodentate HCO_3^- coordination may favor catalysis in small-model complexes and that dissociation energy of M-HCO_3^- may be an important parameter influencing the efficiency.

Catalytic Cycle and Rate-Determining Step. Figure 8 suggests that a main impact of the aza-macrocycle ligand on the catalytic rate constant is the Lewis acidity of the complexed Zn^{2+}. Larger, more electron-donating ligands form weaker Lewis acids, which lead to more "free" hydroxide and bicarbonate ions. One could think that a weakly bound OH^- should make a stronger nucleophile, thereby increasing the rate of CO_2 conversion to HCO_3^-. A more weakly bound bicarbonate would also be expected to make a better leaving group. Therefore strong ligands might be expected to increase the forward rates of Step I and Step II. As a consequence, the Step III deprotonation requires a higher pH, which can effectively mask the higher rate at a given pH.

To quantify the observed trends in Step I, the gas-phase transition state structures were optimized. The associated barrier heights were calculated from an association complex between M-OH^- and CO_2, which places the CO_2 molecule about 2.5 Å above the hydroxide ring and is a minimum on the gas-phase potential energy surface (see Supporting Information). Activation energies were calculated using,

$$E_a \approx E(\mathrm{TS}) - [E(\text{M-}OH^-)\cdots E(CO_2)] \quad (6)$$

The activation energies, E_a, calculated using eq 6 are listed in Table 4, while all optimized coordinates and corresponding energies are provided in the Supporting Information. The transition-state geometries are also shown in Figure 9.

Table 4. Calculated, Counterpoise-Corrected M06-2X/aug-cc-pVTZ//M06-2X/6-311+G(d,p)/B2 Activation Energies for CO_2 Addition, and Calculated M06-2X/aug-cc-pVTZ//M06-2X/aug-cc-pVTZ Adiabatic Bond Dissociation Energies for Bicarbonate Release[a]

	TS(CO_2 addition)	$E_{bond}(HCO_3^-)$
M1	8.53	219.2
M2	5.81	221.2
M3	6.44	225.2
M4	5.65	233.3
M5	6.58	254.1

[a]All values are in kcal/mol.

To verify that the association complex is a true minimum in the aqueous phase, we performed geometry optimizations using the SMD solvation model for the separated reactants and association complexes. The resulting free-energy differences at SMD-optimized structures showed the association complex to be below the separated reactants energetically for all compounds by over 4 kcal/mol, confirming its existence in solution as well as gas-phase.

Interestingly, the gas-phase barrier heights do not follow the same pattern as k_{ind}, particularly between the three-coordinate and four-coordinate structures. The lowest calculated activation energy is for M4, despite it being a less active catalyst than the 4-coordinate structures. The highest calculated activation energy is for M1, in disagreement with k_{ind}. Also, activation energy for M1 is 1.95 kcal/mol higher than for M5, whereas observed k_{obs} is significantly lower for M5, even without pK_a considerations. These observations may be analyzed in terms of the two processes that should govern reactivity of metal-bound hydroxides, as discussed by Anders and co-workers.[47] The calculated transition states consist of one bond being formed, Zn−O(CO_2), and another bond being broken, Zn−O(OH^-). The three-coordinate ligands do not accommodate Zn as tightly, and have less steric shielding, than four-coordinate ligands, allowing better stabilization by CO_2 oxygen lone pairs. This stabilization by CO_2 lowers the calculated E_a for M4 relative to M1−M3. For the same reason, M1 has the highest activation energy despite having the most basic hydroxide because Zn is buried inside the ligand plane. A notable exception is M5, with second highest activation energy despite having the most Lewis acidic Zn. This may be due to the competing trend of OH^- nucleophilicity; M5 has the weakest hydroxide which may be too deactivated to effectively react toward the CO_2 carbon. Separately, M5 also has the largest calculated binding energy for the association complex, increasing E_a, which may be affected by neglect of solvent treatment. Therefore, at least in the gas phase, lower activation energies for CO_2 addition appear to be influenced not only by hydroxide nucleophilicity, but also by stabilization of CO_2 oxygen lone pairs by Zn in the nascent bond. This latter effect should follow the opposite trend of OH^- nucleophilicity. A

dx.doi.org/10.1021/ic300526b | Inorg. Chem. 2012, 51, 6803−6812

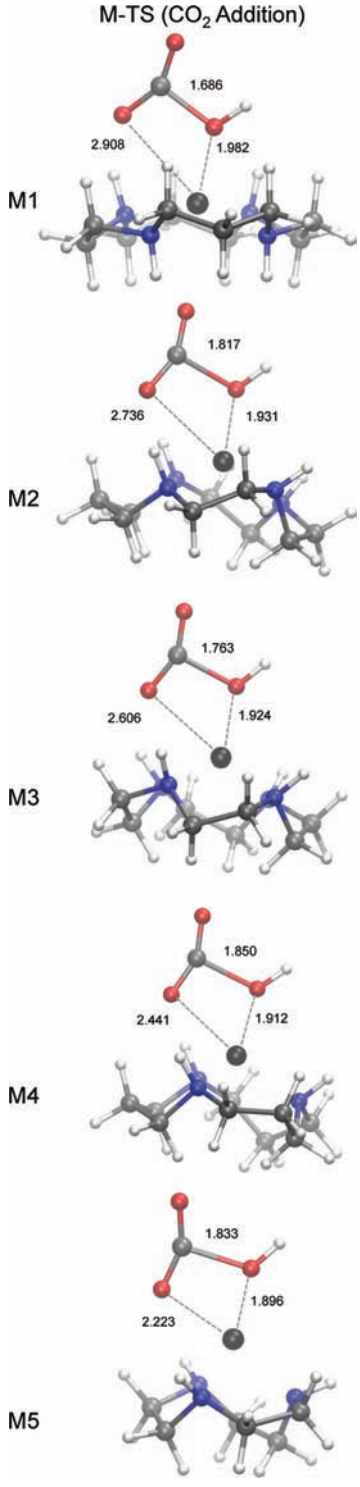

Figure 9. Equilibrium geometries for the first transition state, at M06-2X/6-311+G(d,p)/B2 level. All distances are in Angstroms.

similar analysis based on OH^- charge solid angles of Zn has been proposed to explain reactivity of aza-macrocyclic zinc thiolates by Anders and co-workers.[47] Furthermore, comparison with the experimental rate constants (either k_{ind} or k_{obs}) suggests that CO_2 addition may not be the rate-determining step in the catalytic cycle.

We attempted to estimate activation energies for the second step of the reaction. Dynamical details, including protonation states of the transition states, are not well understood.[12] Previous theoretical work on the bicarbonate release step is limited and suggests a complicated mechanism in which the first water shell is expected to play a critical role. Optimized transition states in the gas phase contain a fully detached HCO_3^- group, interacting through nonbonded interactions with partially formed M-H_2O.[12] Our preliminary calculations of these saddle points found significant coupling of the reaction mode with an intermolecular proton transfer mode between water and fully detached bicarbonate. This proton transfer is requisite in gas-phase treatment but may not be physically relevant in solution. Therefore, a simplified model for the treatment of the bicarbonate release step, utilizing bond dissociation affinities, is considered,

$$M{-}HCO_3^- + H_2O \rightarrow M\text{-}H_2O + HCO_3^- \quad (7)$$

This reaction is depicted by the schematic energy level diagram shown in Figure 10. In the limit of the dissociative (stepwise,

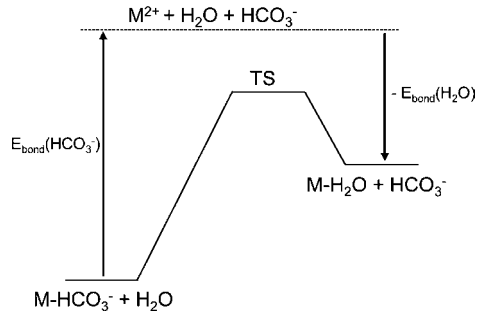

Figure 10. Schematic energy level diagram for the model reaction given in eq 7. The activation energy is decomposed into contributions from corresponding bond dissociation energies.

S_N1) substitution, the activation energy equals the bond dissociation energy of $Zn{-}O(HCO_3^-)$,

$$E_{bond}(M\text{-}HCO_3^-) = E(M\text{-}HCO_3^-) - [E(M^{2+}) + E(M\text{-}HCO_3^-)] \quad (8)$$

In human carbonic anhydrase, a volume profile analysis suggested a dissociative mechanism for this substitution in human CA enzyme.[2] In addition, the mechanism of water exchange in Zn^{2+} in the hexa-aqua complex was found to be dissociative, based on agreement between theoretical calculations and experimental thermochemical data.[48,49] The binding affinity of H_2O (neutral) to Zn^{2+} is significantly lower than that of HCO_3^-. Therefore, this reaction can be expected to be endothermic, and the transition state to be closer to the product, according to the Hammond–Leffler postulate.[50] Indeed, calculated transition state for this step has shown a very late transition state, with a nearly formed $Zn{-}O(H_2O)$ bond and dissociated HCO_3^-.[12] If the reaction is not purely dissociative, the TS will have a dependence on the binding affinity of the nucleophile, which can be partially recovered using the $Zn{-}O(H_2O)$ bond energy,

$$E_a \propto c_1 E_{bond}(M\text{-}HCO_3^-) - c_2 E_{bond}(M\text{-}H_2O) \quad (9)$$

where c_1 and c_2 are coefficients that vary from 0 to 1 and correspond to relative contribution of bicarbonate dissociation and hydroxide association to the transition state. They can be calculated by fitting to a large experimental set of rate constants. On the basis of the above arguments, we assume the activation

dx.doi.org/10.1021/ic300526b | Inorg. Chem. 2012, 51, 6803–6812

energy is related to the Zn−O(HCO_3^-) bond dissociation energy only,

$$E_a \propto E_{bond}(\text{M-HCO}_3^-) \quad (10)$$

The calculated E_{bond} values according to eq 8 are listed in Table 4. The trend in binding energies follows the Zn−O bond lengths and expected Lewis acidity. M1 has the lowest activation energy at 219.2 kcal/mol. Importantly, the three-coordinate complexes are well separated from the four-coordinate ones, in accord with the observed rate constants. M5 has dissociation energy over 20 kcal/mol higher than M1−M4, correctly suggesting that it should have significantly lower rate constant than all the others. For M4 and M5, the higher dissociation energies can be explained by the bidentate binding mode of bicarbonate, so that two Zn−O bonds must be broken. M3 has a lower bond dissociation energy than M2, despite having lower k_{ind} value. This may also be due to the uncertainty of the M3 pK_a, or the fact that the experiments were conducted near the pK_a where pH dependence is large. However, despite the simplicity of the approximation the trend in Zn−O(HCO_3^-) bond dissociaton energies follows the trend in k_{ind} for four out of five compounds. In conjunction with the calculated activation energies for CO_2 addition step, this suggests that bicarbonate release may be the rate-limiting step in CO_2 catalysis by aza-macrocycles. This also highlights mechanistic differences from the enzyme, where the enclosed active site forced shuttling of the excess proton to the bulk solvent is the rate-determining step.

4. CONCLUSIONS

We investigated the catalytic cycle of a panel of five aza-macrocycle ligands in their complex with Zn^{2+}, using high-quality electronic structure methods and validated by stopped-flow measurements. The analysis found that more electron-donating ligands lead to higher intrinsic rate constants, an effect which can be masked by a corresponding increase in the catalytic pK_a. Optimized transition states for the CO_2 addition step were obtained, and showed that the bonding interaction between CO_2 and Zn plays an important role in stabilization of the transition state. This should be useful in designing novel ester hydrolysis catalysts, where dissociation of the leaving group (typically, a bulky ester rather than bicarbonate) may be more favorable. The bond dissociation energy of M-HCO_3^- correlates well with the rate constants, suggesting that bicarbonate release may be the rate-limiting step of the catalytic cycle. The results of this research may be instructive toward designing novel catalysts for CO_2 sequestration applications. In general, it is likely that obtaining rate constants significantly higher than 10^4 M^{-1} s^{-1} operating at pH 9 will require significant contribution from ligand second-coordination spheres, as is the case with CA. For example, assuming that bicarbonate release is rate-limiting, providing hydrogen-bond acceptors in the vicinity of the reactive center (but out of bonding distance of Zn), may lower the bond dissociation energy while having favorable effects on the water pK_a.

■ ASSOCIATED CONTENT

Supporting Information

Coordinates for all minimum and transition state geometries and associated electronic energies; figure depicting reaction coordinate for CO_2 addition, including geometries of association complex, transition state, and product. This material is available free of charge via the Internet at http://pubs.acs.org.

■ AUTHOR INFORMATION

Corresponding Author

*E-mail: lightstone1@llnl.gov (F.C.L.), aines1@llnl.gov (R.D.A.).

Notes

The authors declare no competing financial interest.

■ ACKNOWLEDGMENTS

This work was performed under the auspices of the U.S. Department of Energy by Lawrence Livermore National Laboratory under Contract DE-AC52-07NA27344 with support from Lawrence Livermore National Laboratory (LDRD 10-ERD-035). We thank Laboratory Directed Research and Development for the funding under 10-ERD-035.

■ REFERENCES

(1) Lindskog, S. *Pharmacol. Ther.* **1997**, *74*, 1−20.
(2) Zhang, X.; Hubbard, C. D.; van Eldik, R. *J. Phys. Chem.* **1996**, *100*, 9161−9171.
(3) Behravan, G.; Jonsson, B.; Lindskog, S. *Eur. J. Biochem.* **1990**, *190*, 351−357.
(4) Merz, K. M.; Banci, L. *J. Am. Chem. Soc.* **1997**, *119*, 863−871.
(5) Khalifa, R. G. *Biophys. Chem.* **2003**, *100*, 159−170.
(6) Andersson, I.; Backlund, A. *Plant Physiol. Biochem.* **2008**, *46*, 275−291.
(7) Taylor, T.; Andersson, I. *J. Mol. Biol.* **2008**, *46*, 275−291.
(8) Campbell, I. D.; Lindskog, S.; White, A. I. *J. Mol. Biol.* **1974**, *90*, 469−489.
(9) Silverman, D. N. *Acc. Chem. Res.* **1988**, *21*, 30−36.
(10) Maupin, C. M.; McKenna, R.; Silverman, D. N.; Voth, G. *J. Am. Chem. Soc.* **2009**, *131*, 7598−7608.
(11) Maupin, C. M.; McKenna, R.; Silverman, D. N.; Voth, G. A. *J. Am. Chem. Soc.* **2009**, *131*, 7598−7608.
(12) Mauksch, M.; Brauer, M.; Weston, J.; Anders, E. *ChemBioChem* **2001**, *2*, 190−198.
(13) Looney, A.; Saleh, A.; Zhang, Y.; Parkin, G. *Inorg. Chem.* **1994**, *33*, 1158−1164.
(14) Kumar, V.; Kannan, K. K. *J. Mol. Biol.* **1994**, *241*, 226−232.
(15) Xue, Y.; Vidgren, J.; Svensson, L. A.; Liljas, A.; Jonsson, B. H.; Lindskog, S. *Proteins* **1993**, *15*, 80−87.
(16) Khalifah, R. G. *J. Biol. Chem.* **1971**, *246*, 2561−2573.
(17) Liang, Z.; Xue, Y.; Behravan, G.; Jonsson, B.; Lindskog, S. *Eur. J. Biochem.* **1993**, *211*, 821−827.
(18) Zhang, X.; van Eldik, R.; Koike, T.; Kimura, E. *Inorg. Chem.* **1993**, *32*, 5749−5755.
(19) Zhang, X.; van Eldik, R. *Inorg. Chem.* **1995**, *34*, 5606−5614.
(20) Nakata, K.; Shimomura, N.; Shiina, N.; Izumi, M.; Ichikawa, K.; Shiro, M. *J. Inorg. Biochem.* **2002**, *89*, 255−266.
(21) Brown, R. S.; Salmon, D.; Curtis, N. J.; Kusuma, S. *J. Am. Chem. Soc.* **1982**, *104*, 3188−3194.
(22) Kimblin, C.; Murphy, V. J.; Hascall, T.; Bridgewater, B. M.; Bonanno, J. B.; Parkin, G. *Inorg. Chem.* **2000**, *39*, 967−974.
(23) Huang, D.; Makhlynets, O. V.; Tan, L. L.; Lee, S. C.; Rybak-Akimova, E. V.; Holm, R. H. *Proc. Natl. Acad. Sci.* **2011**, *108*, 1222−1227.
(24) Kato, M.; Ito, T. *Inorg. Chem.* **1985**, *24*, 509−514.
(25) Shengli, G.; Shengming, L.; Yuanqi, Y.; Kaibei, Y. *J. Coord. Chem.* **2011**, *46*, 145−157.
(26) Zhao, Y.; Truhlar, D. G. *Acc. Chem. Res.* **2008**, *41*, 157−167.
(27) Kendall, R. A.; Dunning, T. H., Jr.; Harrison, R. J. *J. Chem. Phys.* **1992**, *96*, 6796−6806.
(28) Amin, E. A.; Truhlar, D. G. *J. Chem. Theory Comput.* **2008**, *4*, 75−85.

(29) Simon, S.; Duran, M.; Dannenberg, J. J. *J. Phys. Chem.* **1996**, *105*, 11024−11031.
(30) Valiev, M.; Bylaska, E. J.; Govina, N.; Kowalski, K.; Straatsma, T. P.; Dam, H. J. J. V.; Wang, D.; Nieplocha, J.; Apra, E.; Windus, T. L.; de Jong, W. A. *Comput. Phys. Commun.* **2010**, *181*, 1477−1489.
(31) Feller, D. J. *J. Comput. Chem.* **1996**, *17*, 1571−1586.
(32) Schuchardt, K. L.; Didier, B. T.; Elsethagen, T.; Sun, L.; Gurumoorthi, V.; Chase, J.; Li, J.; Windus, T. L. *J. Chem. Inf. Model.* **2007**, *47*, 1045−1052.
(33) Kimura, E.; Shiota, T.; Koike, T.; Shiro, M.; Kodama, M. *J. Am. Chem. Soc.* **1990**, *112*, 5805−5811.
(34) Liptak, M. D.; Gross, K. C.; Seybold, P. G.; Feldgus, S.; Shields, G. C. J. *Am. Chem.Soc.* **2002**, *124*, 6421−6427.
(35) da Silva, G.; Kennedy, E. M.; Dlugogorsky, B. Z. *J. Phys. Chem. A* **2006**, *110*, 11371−11376.
(36) Marenich, A. V.; Cramer, C. J.; Truhlar, D. G. *J. Phys. Chem. B* **2009**, *113*, 6378−6396.
(37) Frisch, M. J.; Trucks, G. W.; Schlegel, H. B.; Scuseria, G. E.; Robb, M. A.; Cheeseman, J. R.; Scalmani, G.; Barone, V.; Mennucci, B.; Petersson, G. A.; Nakatsuji, H.; Caricato, M.; Li, X.; Hratchian, H. P.; Izmaylov, A. F.; Bloino, J.; Zheng, G.; Sonnenberg, J. L.;Hada, M.; Ehara, M.; Toyota, K.; Fukuda, R.; Hasegawa, J.; Ishida, M.; Nakajima, T.;Honda, Y.; Kitao, O.; Nakai, H.; Vreven, T.; Montgomery, J. A. Jr.; Peralta, J. E.;Ogliaro, F.; Bearpark, M.; Heyd, J. J.; Brothers, E.; Kudin, K. N.; Staroverov, V. N.;Kobayashi, R.; Normand, J.; Raghavachari, K.; Rendell, A.; Burant, J. C.; Iyengar, S. S.;Tomasi, J.; Cossi, M.; Rega, N.; Millam, J. M.; Klene, M.; Knox, J. E.; Cross, J. B.;Bakken, V.; Adamo, C.; Jaramillo, J.; Gomperts, R.; Stratmann, R. E.; Yazyev, O.;Austin, A. J.; Cammi, R.; Pomelli, C.; Ochterski, J. W.; Martin, R. L.; Morokuma, K.;Zakrzewski, V. G.; Voth, G. A.; Salvador, P.; Dannenberg, J. J.; Dapprich, S.; Daniels,A. D.; Farkas, .; Foresman, J. B.; Ortiz, J. V.; Cioslowski, J.; Fox, D. J. *Gaussian 09*, Revision B.01; Gaussian Inc.: Wallingford, CT, 2009.
(38) Norman, P. R. *Inorg. Chim. Acta* **1987**, *130*, 1−4.
(39) Liang, X.; Weishaupl, M.; Parkinson, J. A.; Parsons, S.; McGregor, P. A.; Sadler, P. J. *Chem.—Eur. J.* **2003**, *9*, 4709−4717.
(40) Tautermann, C. S.; Loferer, M. J.; Voegele, A. F.; Liedl, K. R. *J. Phys. Chem. B* **2003**, *107*, 12013−12020.
(41) Shelton, V. M.; Morrow, J. R. *Inorg. Chem.* **1991**, *30*, 4295−4299.
(42) Harding, A. P.; Popelier, P. L. A. *Phys. Chem. Chem. Phys.* **2011**, *13*, 11264−11282.
(43) Harding, A. P.; Popelier, P. L. A. *Phys. Chem. Chem. Phys.* **2011**, *13*, 11283−11293.
(44) Koike, T.; Kimura, E. *J. Am. Chem. Soc.* **1991**, *113*, 8935−8941.
(45) Subat, M.; Woinaroschy, K.; Gerstl, C.; Sarkar, B.; Kaim, W.; Konig, B. *Inorg. Chem.* **2008**, *47*, 4661−4668.
(46) Rainbolt, J. E.; Koech, P. K.; Yonker, C. R.; Zheng, F.; Main, D.; Weaver, M. L.; Linehan, J. C.; Heldebrant, D. J. *Energy Environ. Sci.* **2011**, *4*, 480−484.
(47) Notni, J.; Gunther, W.; Anders, E. *Eur. J. Inorg. Chem.* **2007**, *2007*, 985−993.
(48) Rotzinger, F. P. *J. Am. Chem. Soc.* **1997**, *119*, 5230−5238.
(49) Hartmann, M.; Clark, T.; van Eldik, R. *J. Am. Chem. Soc.* **1997**, *119*, 7843−7850.
(50) Hammond, G. S. *J. Am. Chem. Soc.* **1955**, *77*, 334−338.